6. A SUMMARY OF RECENT LARGE-SCALE RESEARCH ON HIGH-LIFT DEVICES

By Wallace H. Deckert, David G. Koenig,
and James A. Weiberg
Ames Research Center

SUMMARY

A brief summary of recent 40- by 80-foot wind-tunnel investigations of large-scale models equipped with various high-lift devices is presented. The basic high-lift concepts that were investigated were the externally blown flap, the augmentor wing, and the rotating-cylinder flap. The scope of this paper is limited to a discussion of the wind-tunnel results in terms of maximum lift, descent performance, and pitch trim requirements.

Author

INTRODUCTION

Ames Research Center has a continuing program of developing high-lift devices and determining their effects on aircraft performance, stability, and control characteristics. This paper will summarize three investigations which comprise the most recent work in this area. Two of the high-lift concepts investigated are applicable to jet type STOL aircraft, namely, the externally blown flap and the augmentor wing. The third high-lift concept, the rotating-cylinder flap, may be applicable to any type of aircraft.

The short-field capability of an aircraft is largely a function of the aircraft's ability to fly slowly. For efficient low-speed flight, the requirements are conflicting, that is, to simultaneously provide high lift augmentation and maintain system simplicity. The externally blown flap represents the moderate performance but least complicated approach to the problem. The augmentor wing and the rotating-cylinder flap represent the high performance but relatively complex approach.

Wind-tunnel results of these investigations will be examined from the standpoint of maximum lift, descent performance, and pitch trim requirements. Other performance characteristics peculiar to each of the high-lift devices will be discussed.

NOTATION

b wing span, ft

c wing chord parallel to plane of symmetry, ft

c_{ref}	reference chord, ft
C_D	drag coefficient, $\frac{drag}{q_o S}$
C_J	jet thrust coefficient, $\frac{gross\ thrust}{q_o S}$
C_L	lift coefficient, $\frac{lift}{q_o S}$
ΔC_{L_f}	incremental lift coefficient due to flap deflection at $\alpha = 0^o$, $C_L - (C_L)_{\delta_f=o}$
$(C_m)_{o.25c_{ref}}$	pitching-moment coefficient, $\frac{M}{q_o S c_{ref}}$
ΔC_{m_f}	incremental pitching-moment coefficient due to flap deflection at $\alpha = 0^o$, $C_m - (C_m)_{\delta_f=o}$
C_{μ_f}	flap BLC blowing-momentum coefficient, $\frac{flap\ nozzle\ thrust}{q_o S}$
q_o	free-stream dynamic pressure, lb/sq ft
S	wing area, sq ft
T/W	thrust/gross weight ratio, $\frac{C_J}{C_L}$
T_c'	propeller thrust coefficient, $\frac{thrust}{q_o S}$, where thrust is the total thrust of two propellers
V	free-stream velocity or scaled airspeed as noted, knots
V_s	stall speed, knots
$\frac{U}{V}$	velocity ratio for rotating cylinder, $\frac{cylinder\ surface\ speed}{free\text{-}stream\ velocity}$
W	gross weight, lb
α	geometric angle of attack of fuselage reference line, deg
δ_a	aileron deflection relative to wing chord, deg
δ_f	flap deflection relative to wing chord, deg

$\delta_{f_{AFT}}$ flap deflection of aft segment of a flap relative to chord of forward segment of the flap, deg

$\delta_{f_{AUX}}$ flap deflection of added auxiliary flap relative to chord of basic flap, deg

DESCRIPTION OF THE MODELS

Model With an Externally Blown Flap

A cross section of the externally blown flap configuration that was investigated is shown in figure 1. A J-85 turbojet was installed in the underslung nacelle, with the thrust axis of the J-85 set parallel to the wing chord. A paddle deflector was placed at the exit of the standard round exhaust pipe. The paddle deflector was deflected, trailing edge up, to deflect the hot exhaust gases toward the wing trailing edge and through the flap slot for blowing boundary-layer control. The main or forward flap segment had a chord of 0.22. A small auxiliary flap was added to the main flap. A 0.15 c slat was installed on the wing leading edge.

A photograph of the model installed in the 40- by 80-foot wind-tunnel test section is shown in figure 2. The wing had an aspect ratio of 5.4 and a span of 36.6 feet with the quarter-chord line swept about 35°. The slat was installed full-span across the wing leading edge, except for cutouts for the nacelles. The trailing-edge flaps were installed from 11 to 63 percent of the wing semispan. The horizontal tail was located 1.16 $\bar{c}$ above the wing chord plane, with a tail length of 2.68 $\bar{c}$ and a volume coefficient of about 0.65.

Model With an Augmentor Wing

A cross section of the augmentor wing configuration that was investigated is shown in figure 3.

Primary air was ducted spanwise along the wing and ejected through the primary nozzle. The augmentor wing is essentially an ejector system with the forward wall formed by the wing, fixed vane, and lower door, with the rear wall formed by the upper door and trailing-edge flap. Primary air draws in secondary air from the wing upper surface and the mixed jet is ejected downward between the flap and lower door. A flap BLC system was incorporated. The primary air for flap BLC was also augmented. An inlet for secondary air was provided in the lip of the augmentor upper door. Secondary air flowed through the slot in the upper door and the mixed flow was ejected over the flap knee. The deflection of the upper door lip could also be adjusted as required to maintain attached flow over the outer surface of the upper door. A 15-percent chord slat was installed on the wing leading edge.

Figure 4 is a photograph of the model installed in the 40- by 80-foot test section. The straight wing had an aspect ratio of 8.0 and a span of 42.2 feet. The augmentor extended from 12.5 to 72 percent of the wing

semispan. Blown ailerons extended from 72 percent of the wing semispan to the wing tips. The leading-edge slat extended from the fuselage to the wing tip as shown. The inlet in the nose of the fuselage was for a J-85 gas generator. Hot gases from the J-85 powered the turbines of modified Viper engines and were expelled through the tail pipes located in the aft section of the fuselage as shown in the photograph. The two inlets on the side of the fuselage were for the modified Viper engines. The Viper compressor output was directed to the augmentor primary nozzle and to the aileron BLC system. Primary air for the flap BLC system was supplied by J-85 compressor bleed.

Model With a Rotating-Cylinder Flap

A rotating-cylinder flap was installed on an existing model as shown in figure 5. The cylinder was installed full-span across the trailing edge of the wing. The cylinder on each semispan was composed of two segments with an electric motor driving each. The large diameter disks on the cylinder are end plates for each cylinder segment (the outboard disk is hidden behind the wing tip end plate). The semispan of the cylinder, as viewed in figure 5, was 11 feet. Cylinder diameter was 10.9 inches (0.13 c), and the surface of the cylinder was of smooth aluminum. The insert in figure 5 shows that the cylinder was placed within the leading-edge contour of the flap and that the flap included a slotted aft segment. Flap chord, including the cylinder, was 0.46 c. A full-span slat with a chord of 0.22 c was installed on the leading edge of the wing.

A photograph of the model installed in the wind tunnel is shown in figure 6. The 9.3-foot diameter propellers were driven by electric motors. The straight wing had an aspect ratio of 3.5 and a span of 25 feet.

A 44-percent chord conventional flap was also evaluated on the model shown in figure 6. A cross section of this double-hinged plain flap is shown in figure 7.

TEST AND PROCEDURE

Model With an Externally Blown Flap

The investigation was conducted at Reynolds numbers of 4.3 to 8.2 million based on the wing mean aerodynamic chord of 7.96 feet, which corresponded to free-stream dynamic pressures of 8.5 to 32 psf. The tests were conducted with the horizontal tail set at 0° incidence. The lift and drag coefficients are untrimmed gross coefficients that include the thrust of the J-85 turbojet engines. The engine gross thrust was determined from total pressure probes placed in the exhaust pipe. The mean aerodynamic chord is the reference chord for this model.

The model was mounted on struts as shown in figure 2. Small drag corrections were applied to the data to account for the tail strut which was largely

unfaired (strut forces on all faired portions of the struts were isolated from the model). Standard wind-tunnel wall corrections were applied.

Model With an Augmentor Wing

The investigation was conducted at a free-stream tunnel velocity of about 49 knots (q_o = 8, Reynolds number = 4.9 million based on the wing root chord of 5.67 ft). Test results presented in this paper were conducted with the horizontal tail off. The lift and drag coefficients are untrimmed net aerodynamic coefficients excluding residual thrust in the J-85 exhaust and inlet ram drag. The jet thrust coefficient, C_J, is based on the augmented or "effective" jet thrust of the augmentor measured at q_o = 0 plus the thrust due to BLC on the ailerons. Aileron BLC thrust was about 3 percent of the augmentor thrust. Blowing rates were adjusted by varying J-85 power, with aileron BLC being used continually for all power-on testing, and flap BLC was controlled as desired through a remotely actuated valve controlling J-85 bleed supply. The wing root chord is the reference chord for this model.

The model was mounted on faired struts (fig. 4) in a manner which isolated the strut forces from the model. Standard wind-tunnel wall corrections were applied to the basic power-off, clean configuration.

Model With a Rotating-Cylinder Flap

The investigation was conducted at free-stream tunnel velocities from 30 to 40 knots (q_o = 2.6 to 5.0, Reynolds number = 2.0 to 2.9 million based on the wing mean aerodynamic chord of 7.0 ft). Test results are presented for a wing-body configuration with no empennage. The lift and drag coefficients are untrimmed gross coefficients that include propeller thrust. The propeller thrust characteristics were determined by wind-tunnel tests with the propellers on and off the model. The mean aerodynamic chord is the reference chord for this model.

The model was mounted on faired struts (fig. 6) in a manner which isolated the strut forces from the model. Wind-tunnel wall corrections were not applied.

RESULTS AND DISCUSSION

Model With an Externally Blown Flap

Typical lift-drag polars are presented in figure 8 for thrust coefficients (C_J) of 0, 0.5, and 1.36 which was the highest thrust coefficient evaluated. The polars on the left-hand side of figure 8 are for a flap deflection $\delta_f/\delta_{f_{AUX}}$ of $10^o/20^o$, which was the smallest flap deflection evaluated. For C_J of 1.36, a maximum lift coefficient of 3.4 was obtained at a maximum descent angle of 4^o. For descent, large flap deflections are of interest and

the polars on the right-hand side of figure 8 are for a flap deflection of 40°/40°, which was the largest flap deflection evaluated. For C_J of 1.36, a maximum lift coefficient of 4.3 was obtained at a maximum descent angle of about 13° and an angle of attack of 25°. At 0° angle of attack, a comparison of the data obtained at C_J values of 0 and 1.36 shows that the incremental lift coefficient due to blowing was 1.8. If deflected thrust were used or flap turning efficiency were 100 percent, ΔC_L would be 1.36. Thus of the incremental lift coefficient of 1.8, 75 percent could be provided by the jet reaction. The flap actually converted only 43 percent of the jet reaction to lift so that the circulation and jet lift were nearly equal.

The pitching-moment coefficient for the untrimmed maximum lift coefficient (4.3) was -1.3. This corresponds to a trimmed value of maximum lift coefficient of 3.82 which represents a lift loss of about 11 percent due to trim requirements (static margin was 40 percent). Engine operation and flap deflection did not effect static margin or shift the pitching-moment curve.

Figure 9 illustrates the feasibility of direct flight path control with a rapidly responding small auxiliary flap. Flight path angle, in both climbing and descending flight, is presented against flight speed for an assumed wing loading of 70 pounds per square foot and a constant thrust/weight ratio of 0.4, with flight speed based on a 20-percent margin from trimmed stall speeds. Lines indicate the main flap deflections evaluated 10°, 20°, and 40°; the dashed line is for 30° added by interpolation. Auxiliary flap deflections from 20° to 40° were evaluated, which is the primary variable along any one line as shown. Changes in angle of attack for a given main flap deflection are small. Angle of attack varied from 7° to 11° for a flap deflection change from 40°/40° to 10°/20°. Figure 9 shows that auxiliary flap deflection changes of 20° produced flight path changes of about 4°. Flight path changes of 6° or more appear to be attainable by increasing the deflection range of the auxiliary flap, say from 0° to 50°. For example, for a main flap deflection of 30°, at constant speed and constant thrust, direct flight path control from about a 4° descent angle to a 2° climb angle appears feasible for this configuration.

Model With an Augmentor Wing

Prior to the wind-tunnel investigation, the static performance of the augmentor was measured on the Ames static test stand. Static runs were conducted with the augmentor upper door and trailing-edge flap removed and with these components installed as shown in figure 3. It was found that the primary nozzle thrust was augmented about 40 percent.

Lift coefficient as a function of flap deflection is shown in figure 10 for 0° angle of attack and for an augmented thrust coefficient of 0.81. For all the tests, the upper and lower door positions were adjusted to optimum positions as indicated by the static test results. Figure 10 shows that maximum lift increments due to flap deflection would be obtained at a flap deflection of 80°. The figure also shows that the use of BLC and aileron droop are effective in producing significant lift increments for all the flap settings considered.

Typical lift-drag polars for the augmentor wing configuration are presented in figure 11. The lift and drag coefficients are net aerodynamic coefficients, that is, the combined ram drag of all inlets and small residual thrust of the J-85 exhaust are not included. The polars on the left-hand side of figure 11 are for a flap deflection of 60° with the ailerons drooped 45°. Polars are shown for augmented thrust coefficients of 0, 0.81, and 1.30, which was the highest value investigated, with no blowing at the flap knee. One polar is shown with flap BLC. Figure 11 shows that a maximum lift coefficient of 6 was obtained which, for comparison, is about the same for propeller-driven aircraft with effective large-chord mechanical flaps - such as the Breguet 941 STOL aircraft. At 0° angle of attack, a comparison of the data obtained at C_J values of 0 and 1.30 shows that the lift coefficient increment due to augmentor thrust was 2.4 compared to the vertical component of the augmented thrust of 1.1. Thus over half the lift coefficient increment was due to circulation lift. Blowing over the flap knee with a blowing momentum coefficient of 0.04 increased the lift coefficient by about 0.5 (about a 10-percent increase in maximum lift coefficient). For this configuration, maximum descent angles were 6° to 7°. The effect of increasing the flap and aileron deflections is shown on the right-hand side of figure 11 for a thrust coefficient of 0.81 with flap BLC. The polar for a flap deflection of 60° and aileron deflection of 45° is repeated from the left-hand side of figure 11 for convenience. It is compared to a polar for a flap deflection of 100° and an aileron deflection of 70°. Maximum lift coefficients for both configurations were about the same. The additional drag due to the higher flap and aileron deflections increased the maximum descent angle from about 7° to 12°.

The investigation showed that the pitching moments for the augmentor wing were relatively low. In figure 12, flap lift coefficient is presented against flap lift coefficient divided by flap pitching-moment coefficient for 0° angle of attack. Figure 12 thus shows the lift that was realized for a given pitching moment. Typical jet flap values obtained from references 1 and 2 are shown for comparison. The augmentor wing configuration, compared to the jet flap, produced about twice the lift for a given pitching moment.

Model With a Rotating-Cylinder Flap

Cylinder speed and power requirements are presented in figure 13. On the left-hand side of the figure, lift coefficient is plotted against a velocity ratio. The velocity ratio is the surface speed of the cylinder, made dimensionless by reference to free-stream velocity. Shown, for a flap deflection of 60° with an additional 18° deflection of the aft flap, are curves for propeller thrust coefficients of 0 with an angle of attack of 0°, and a thrust coefficient of 4 with an angle of attack of 16°. The propeller thrust coefficient, T_c', is referenced to free-stream dynamic pressure and wing area. At low velocity ratios, the flow over the surface of the flap was separated. As cylinder speed was increased, the boundary layer was energized to a greater degree, and thus the separated area on the flap was progressively reduced. At the knee of the curves, which corresponds to a velocity ratio of about 5, flow became fully attached. Velocity ratios greater than about 5 increased lift only slightly. As indicated by these two curves, it was found that the velocity ratio required for attached flow was independent of both propeller thrust

coefficient, that is, propeller slipstream effects, and angle of attack. The curve on the right-hand side of figure 13 shows the horsepower required to rotate the cylinder as a function of both velocity ratio and cylinder RPM. The horsepower is the total horsepower required by the cylinder including both frictional horsepower and air horsepower. The curve is for a free-stream velocity of 40 knots. For a velocity ratio of 5, corresponding to about 7000 RPM, 15 horsepower was required. The total length of the cylinder was 22 feet. Thus the power required to energize the boundary layer to achieve fully attached flow was less than 1 hp per foot of cylinder length.

Typical lift-drag polars for the rotating-cylinder flap are presented in figure 14 for a velocity ratio of 6.6. On the left-hand side of figure 14, the solid lines are for the rotating-cylinder flap deflected $60^\circ/18^\circ$ and thrust coefficients of 0 and 4. For comparison, the dashed lines are for the same model, without a rotating cylinder, and with the double-hinged plain flap deflected $60^\circ/30^\circ$. For $T_c' = 0$, and a wing of aspect ratio 3.5, a maximum lift coefficient of 4 was obtained for the rotating-cylinder flap, compared to a value of about 3 for the double-hinged flap. For a thrust coefficient of 4, a maximum lift coefficient of 9.1 was obtained for the rotating-cylinder flap, compared to 7.5 for the double-hinged flap. A maximum lift coefficient of 9.1, for example, corresponds to a 38 knot stall speed at a wing loading of 45 pounds per square foot. The drag value for this maximum lift point corresponds to a maximum descent angle of about 14°. The polars on the right side of figure 14 show that significantly higher drag values, as well as higher lift values, were obtained by increasing the deflection of the main flap to $70^\circ/18^\circ$, with maximum lift occurring at a descent angle of nearly 20°.

The flap lift and moment increments for the model with a rotating-cylinder flap are presented in figure 15 for 0° angle of attack. Incremental flap lift coefficient is plotted against flap lift coefficient divided by flap pitching-moment coefficient. Results for the basic model with the double-hinged flap are shown for reference. Two sets of results are shown for the rotating-cylinder flap, for two different wing-flap configurations. The lower curve is for the flap hinge near the lower surface of the wing, which was the configuration selected for the presentation of results in figures 13 and 14. The upper curve is for a second configuration with the flap hinge located near the wing upper surface. It is seen that the lift obtained for a given pitching moment is significantly higher for the rotating-cylinder flap, compared to the values for the double-hinged flap. And, for the rotating-cylinder flap, lift per unit pitching moment was found to be much greater for the flap hinge located at the upper surface. Lift coefficients for both hinge positions were approximately equal.

CONCLUDING REMARKS

Wind-tunnel investigations of large-scale models equipped with an externally blown flap, an augmentor wing, and a rotating-cylinder flap have been briefly reviewed.

For the model with the externally blown flap, wind-tunnel results show a maximum lift coefficient of 4.3 was obtained for a thrust coefficient of 1.36 and indicate the feasibility of utilizing a small rapidly responding auxiliary flap for direct flight path control.

For the model with an augmentor wing, an augmentation ratio of 1.4 was obtained; for an augmented thrust coefficient of 1.30, a maximum lift coefficient of 6 was obtained which is similar to the maximum lift coefficient achieved by present propeller-driven STOL aircraft; and one problem generally associated with the jet flap concept, namely, the existence of large pitching moments at high lift coefficients, was found to be significantly reduced.

For the model with a rotating-cylinder flap, a maximum lift coefficient of 9.1 was obtained for a thrust coefficient of 4, the power required to energize the boundary layer was found to be low, and pitching moments were found to be significantly less than those for a plain double-hinged flap.

REFERENCES

1. Butler, S. F. J.; Moy, B. A.; and Hutchins, G. D.: Low-Speed Tunnel Tests of an A. R. 9 Jet-Flap Model, With Ground Simulation by Moving-Belt Rig. R.A.E. TN Aero. 2957, 1964.

2. Gainer, Thomas G.: Low-Speed Wind Tunnel Investigation to Determine the Aerodynamic Characteristics of a Rectangular Wing Equipped With a Full-Span and an Inboard Half-Span Jet-Augmented Flap Deflected 55°. NASA MEMO 1-27-59L, 1959.

EXTERNALLY BLOWN FLAP CONFIGURATION

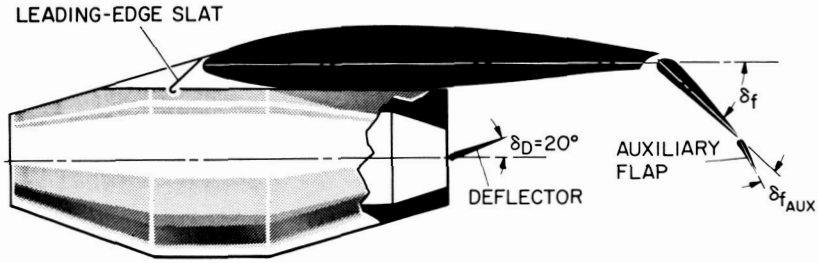

WING ASPECT RATIO = 5.4
HALF-SPAN FLAPS

Figure 1

WIND-TUNNEL MODEL WITH EXTERNALLY BLOWN FLAPS

Figure 2

A-34818.1

AUGMENTOR WING

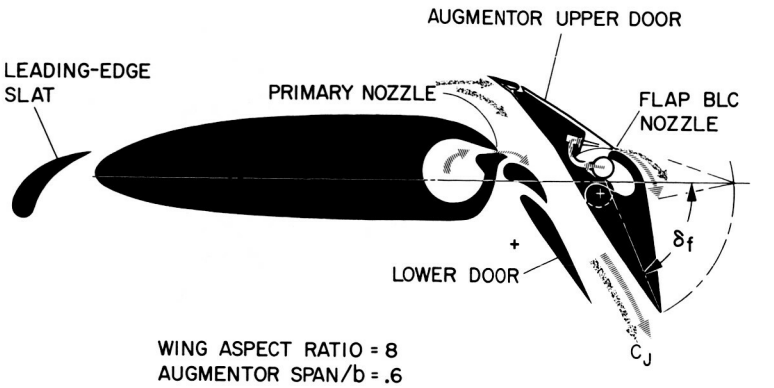

Figure 3

WIND-TUNNEL MODEL WITH AN AUGMENTOR WING

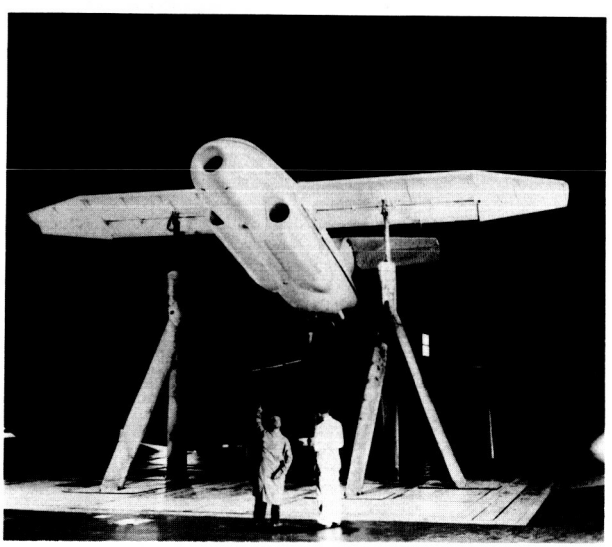

Figure 4 A-35855.1

SIDE VIEW OF ROTATING-CYLINDER FLAP

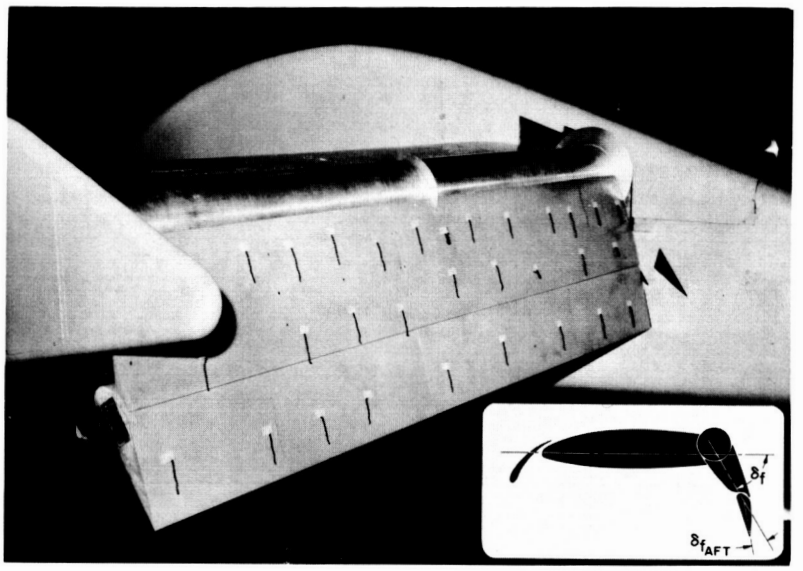

Figure 5 A-35913.1

WIND-TUNNEL MODEL WITH ROTATING-CYLINDER FLAP

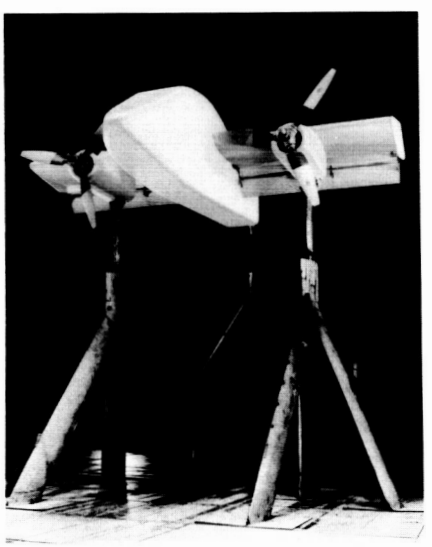

Figure 6 A-35912.1

DOUBLE-HINGE PLAIN FLAP

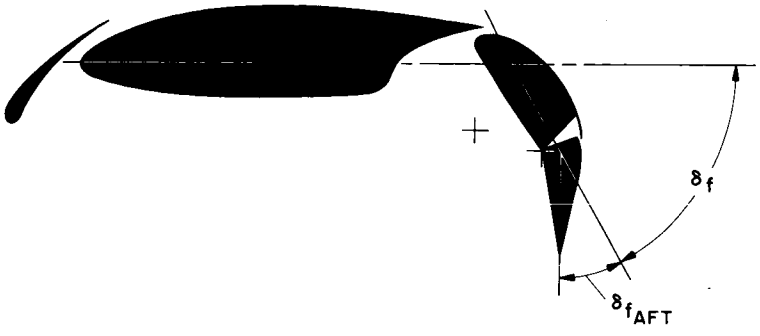

Figure 7

LIFT-DRAG POLARS FOR EXTERNALLY BLOWN FLAP

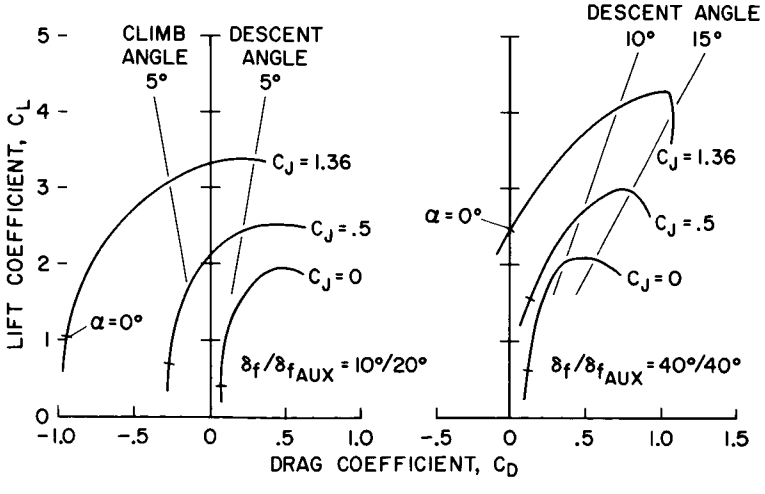

Figure 8

FLIGHT PATH CONTROL WITH AUXILIARY FLAP

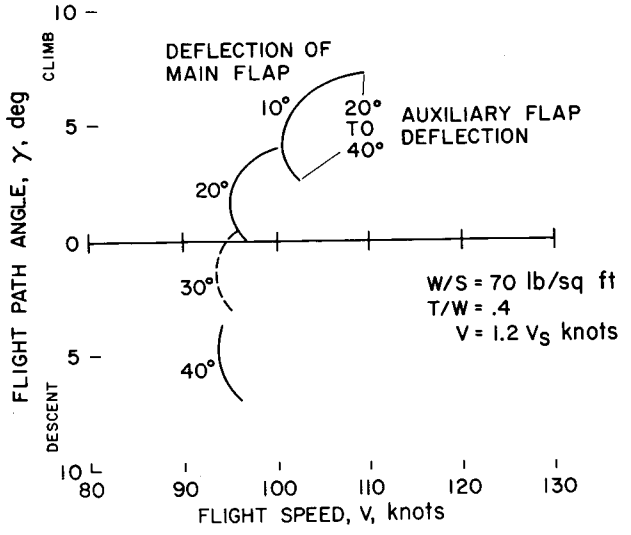

Figure 9

EFFECT OF FLAP AND AILERON DEFLECTION ON LIFT COEFFICIENT

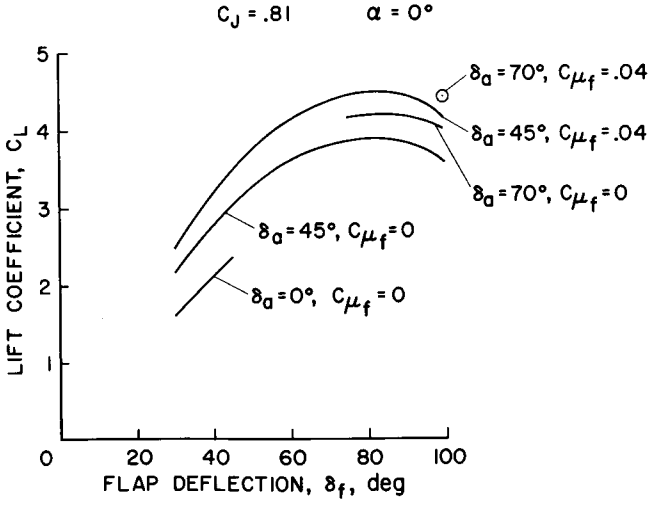

Figure 10

LIFT - DRAG POLARS FOR AUGMENTOR WING

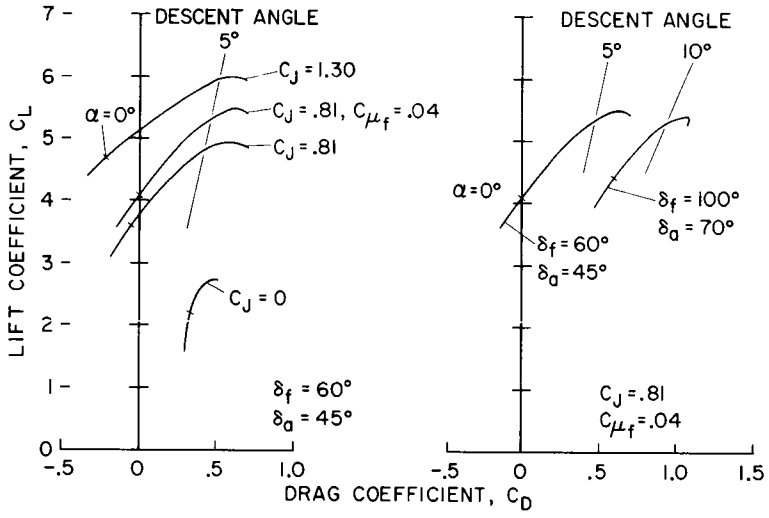

Figure 11

FLAP LIFT AND MOMENT INCREMENTS FOR AUGMENTOR WING

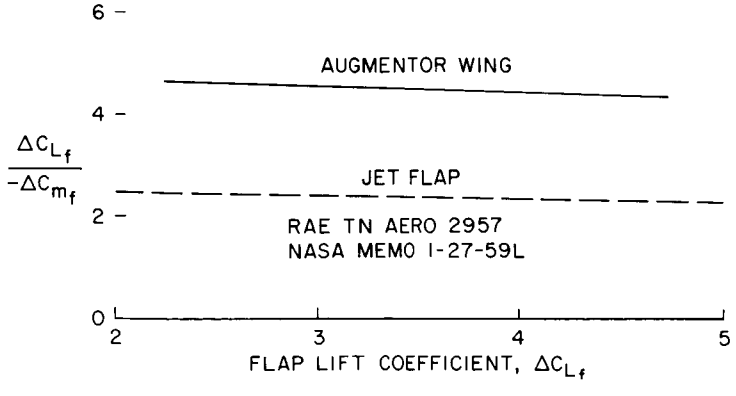

Figure 12

CYLINDER SPEED AND HORSEPOWER REQUIREMENTS

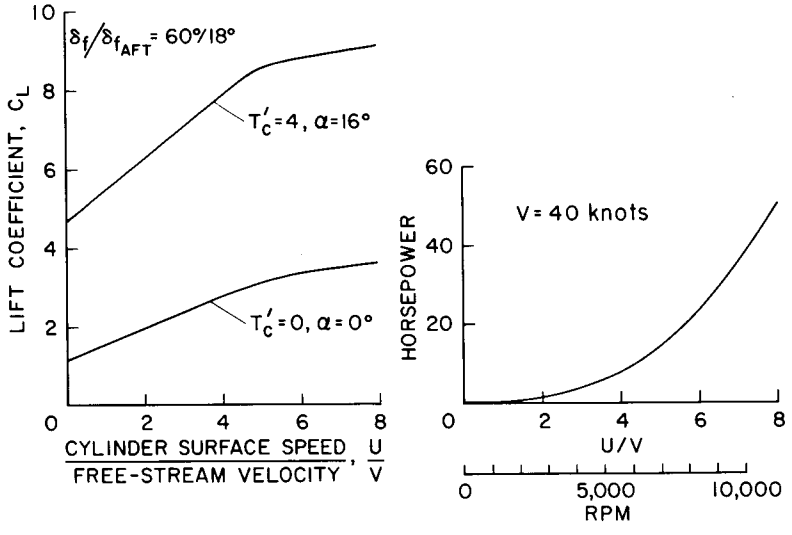

Figure 13

LIFT-DRAG POLARS FOR ROTATING-CYLINDER FLAP
U/V=6.6

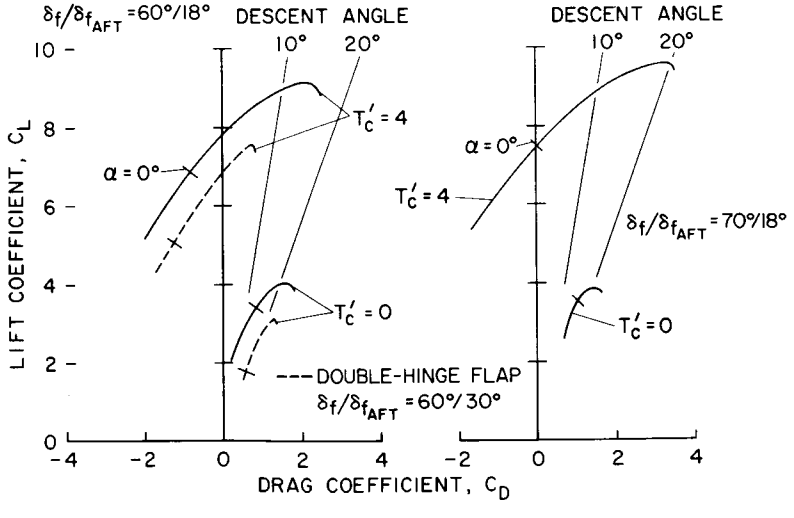

Figure 14

FLAP LIFT AND MOMENT INCREMENTS FOR ROTATING-CYLINDER FLAP

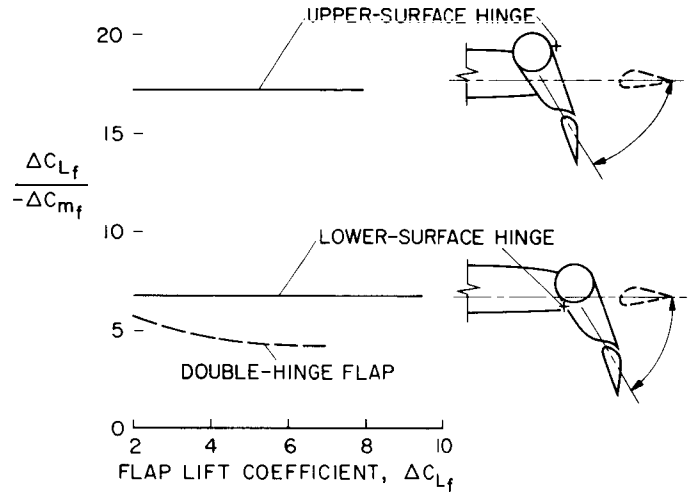

Figure 15